



Bimetal-phthalocyanine based covalent organic polymers for highly efficient oxygen electrode

Zhijian Liao, Yalan Wang, Qiuli Wang, Yuanhui Cheng*, Zhonghua Xiang*

State Key Lab of Organic-Inorganic Composites, College of Chemical Engineering, College of Energy, Beijing University of Chemical Technology, Beijing 100029, PR China



ARTICLE INFO

Keyword:

Covalent organic polymers
Oxygen reduction/evolution reaction
Molecular design
Metal-air battery

ABSTRACT

The feature of tunable constituents in covalent organic polymers (COPs) via combination of predesigned building units is of great interest in exploring multi-functional catalysts. Here, we report constituent-tunable metal-phthalocyanine-based covalent organic polymers as self-sacrificial precursors for fabrication of mono- (Fe or Ni) and bi-metallic (Fe-Ni) heteroatoms/carbon catalysts toward both oxygen reduction reaction (ORR) and oxygen evolution reaction (OER). As a result, the as-prepared FeNi-COP-800 exhibits an efficient ORR performance with a half-potential of 0.80 V as well as an IrO_2 -like OER activity with a potential of 1.63 V at 10 mA cm⁻², which surpass those of monometallic Fe-COP-800 and Ni-COP-800. Moreover, a zinc-air flow battery using FeNi-COP-800 catalyst not only shows a higher power density than the battery using Pt/C-IrO₂/C but also displays superior stability with 2.90% potential loss after 85 cycles in 175 h of practical operation. Accordingly, this work provides a facile but efficient approach in molecular incorporation of desired constituents to obtain bi/multi-active sites in a single catalyst for various catalytic roles, including, but not limited to, oxygen reduction, hydrogen evolution, oxygen evolution.

1. Introduction

Electrocatalysts toward oxygen reduction and evolution reaction (ORR and OER) play a significant role in sustainable energy technologies such as rechargeable metal-air batteries [1–8]. However, single electrocatalyst that can simultaneously drive both efficient ORR and OER is difficult to achieve because both processes do not share similar reversible reaction pathways and activation free energies [9–11]. For example, Pt- and Ru/Ir-based catalysts are respectively regarded as ORR and OER benchmark but inferior OER and ORR performance [12–16], while such single catalytic activity in these catalysts makes them unfavorable as bi-functional oxygen electrocatalyst in rechargeable metal-air battery [17,18]. Therefore, an urgent development of efficient electrocatalysts with dual/multi-active sites for satisfying both ORR and OER processes is highly desirable.

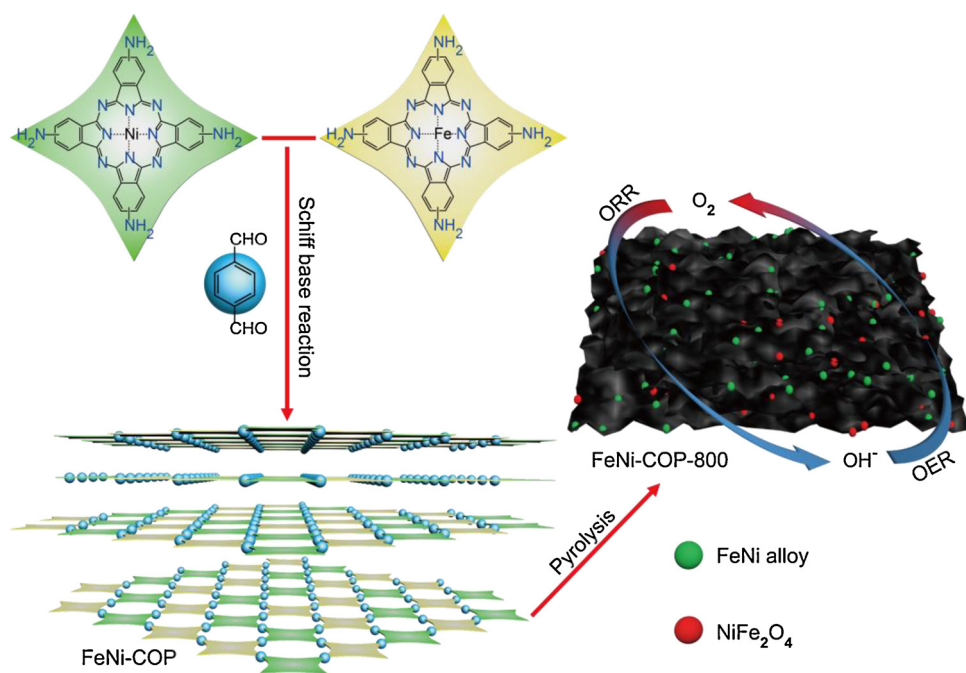
In the past decade, many investigations have pointed to Fe/nitrogen dual-doped carbon (Fe/N-C) as the most promising candidates for highly efficient ORR catalytic activity, owing to the catalytic active sites of pyridinic–N and Fe–N_x [19–21]. On the other hand, thanks to the easy formation of Ni-O bond between Ni atom and water molecule, OER processes can be well-accelerated consequently, which trigger that the metal nickel- or nickel oxide-based materials are the most effective substitutes for superior OER catalytic activities in alkaline solution

[22–26]. Although incorporating iron into nickel catalysts can efficiently enhance OER performance and the catalytic stability, the poor performance toward ORR in these catalysts is still far away from meeting the requirements of metal-air batteries [27–29]. Additionally, Nickel-iron catalysts easily meet the degradation at high temperatures, which made it difficult to fabricate active nickel-iron catalysts via pyrolysis methods. [30,31]. Thus, a huge interest is how dual/multi-active sites toward both ORR and OER can be desirably tailored into a single electrocatalyst by an ideal method. So far, the typical methods for fabricating ORR-OER bi-functional materials involve mixing the sources of transition metal (TM), heteroatom (HA) and carbon, followed by pyrolysis [32–36]. Such random mixture generally induces that TM and HA sources are disorderly dispersed on carbon frameworks, which furtherly makes them hard to achieve the anchoring of the active sites [33,35]. Therefore, rational design in precursors is also of great benefit for the ordering formation of catalytic sites in carbon matrix.

Most recently, Covalent organic polymers (COPs), as a novel class of self-sacrificial precursors for *in situ* generating carbon-supported catalysts owing to the rich carbon element in COPs [37–39], have gained increasing attention due to some properties such as well-defined chemical composition and interconnectivity of building blocks in various dimensions, and versatility in molecular design [40,41]. Attractively,

* Corresponding authors.

E-mail addresses: chengyh@mail.buct.edu.cn (Y. Cheng), xiangzh@mail.buct.edu.cn (Z. Xiang).



Scheme 1. Schematic illustration for the preparation of FeNi-COP-800.

the selection of appropriate building units for COPs can atomically control the integration of the building units to tune the components and functions [42,43], and the directionality of covalent bonds provides a means of precisely controlling how building units come together into predesigned precursors with rigid structures [44], which would serve as an attractive method for the design and fabrication of COP-derived electrocatalysts with orderly dispersing dual active sites on carbon matrix for satisfying both ORR and OER.

Herein, we reported constituent-tailorable Fe/Ni-phthalocyanine-based covalent organic polymers (Fe/Ni-COPs) as self-sacrificial precursors to fabricate mono- (Fe- or Ni-) and bi-metallic (FeNi-) heteroatoms/carbon catalysts (denoted as Fe/Ni-COP-X, X represents pyrolysis temperature) for both ORR and OER (**Scheme 1**). By appropriately controlling the integration of different building units to tune the components in Metal-COP materials, we found that FeNi-COP-800 catalyst exhibits the best ORR and OER activities among all the as-prepared Fe/Ni-COP-X catalysts, which is closely associated with the coexistence of Fe and Ni elements in FeNi-COP-800. Additionally, FeNi-COP-800 exhibits an efficient ORR performance with a half-potential of 0.80 V as well as an IrO₂-like OER activity with a potential of 1.63 V at 10 mA cm⁻², which significantly surpass those of monometallic Fe-COP-800 and Ni-COP-800 catalysts. Furthermore, a zinc-air flow battery comprising FeNi-COP-800 catalyst shows a power density of 64 mW cm⁻² and superior stability with 2.9% potential loss after 85 cycles in 175 h of practical operation. Therefore, this work on appropriately tuning the building units with desired components for COP precursors might provide a simple way in rational design of electrocatalyst with bi/multi-active sites to achieve various catalytic roles.

2. Materials and methods

2.1. Materials

4-nitrophthalonitrile (AR, 99.0%), KOH (AR, ≥ 90%) and NaOH (AR, ≥ 90%) were purchased from Aldrich. H₂SO₄ (AR, ~98%), 20% Pt/C, IrO₂, carbon black, *N,N*-dimethylacetamide (DMAc, 99.5%), *N,N*-dimethylformamide (DMF, 99.8%) and tetrahydrofuran (THF, 99.5%) were purchased from J&K scientific Ltd. Na₂S·9H₂O (AR, ≥ 98%), NiCl₂ (AR, ≥ 98%), FeCl₃ (AR, ≥ 98%) and terephthalaldehyde (TA, 99%)

were purchased from energy chemical. All the chemical reagents have been used without further purification.

2.2. Synthesis of metal tetraaminophthalocyanine (MePc(NH₂)₄)

MePc(NH₂)₄ (FePc(NH₂)₄ and NiPc(NH₂)₄) were prepared according to the published method with slight modification [45]. General procedure for synthesis of MePc(NH₂)₄ is given as follows. A finely ground mixture of 4-nitrophthalonitrile (20 mmol), *MgCl*₂ (5 mmol), urea (9.6 g, 160 mmol) and a catalytic amount of ammonium molybdate was reacted in solid state at 160 °C for 5 h. The resulting solid product was ground and further stirred in 1 M aqueous HCl solution (300 mL) and 1 M aqueous NaOH solution (300 mL) at 90 °C for 1 h, respectively. The residue was then filtered, washed with water to remove the intermediates and unreacted components, and dried under vacuum to obtain MePc(NO₂)₄. The as-synthesized MePc(NO₂)₄ (2 mmol) was further converted to MePc(NH₂)₄ by reaction with Na₂S·9H₂O (40 mmol) in DMF (30 mL) at 60 °C for 8 h. The solution was then poured into water (120 mL), and the precipitate was collected by centrifugation, repeatedly washed with water until neutral condition. The product was dried under vacuum to get blackish-green MePc(NH₂)₄ in 45% isolated yield.

2.3. Synthesis of FeNi-phthalocyanine-based COP (FeNi-COP)

The preparation of FeNi-phthalocyanine-based covalent organic polymer is based on the schiff base reaction, and the procedure is given as follows. A 250 mL flask containing DMAc (90 mL) solution FePc(NH₂)₄ (0.6 mmol), NiPc(NH₂)₄ (0.4 mmol) and TA (2 mmol) was air-removed by N₂ for 30 min, and then was heated at 150 °C for 72 under N₂ protection. After the mixture is cooling to room temperature, the precipitate was collected by filtration, washed with DMAc and THF for several times, extracted by Soxhlet with THF for 24, and dried at 120 °C under vacuum overnight to give the product as dark green powder in 72% isolated yield.

2.4. Synthesis of FeNi-COP-derived catalyst

The as-obtained FeNi-COP was then calcined in various temperature

to gain the FeNi-COP-X, where X represents pyrolysis temperatures in 700 °C, 800 °C and 900 °C. Generally, FeNi-COP was heated from room temperature to 350 °C for 2 h at a rate of 5 °C min⁻¹ in an Ar atmosphere, and subsequently in a rate of 5 °C min⁻¹ heating up to the desired temperature such as 800 °C for another 2 h to obtain FeNi-COP-800. Furthermore, 1 M H₂SO₄ was used to treat FeNi-COP-800 to gain Acid-treated FeNi-COP-800 for contrast experiment.

2.5. Material characterization

A Nicolet NEXUS 670 Fourier transform infrared spectrometer was used to record IR spectra in the 4000–400 cm⁻¹ range. Solid-state NMR spectra was measured in a Bruker AV300 spectrometer operating at 75.5 MHz for ¹³C. Powder X-ray diffraction (PXRD) was performed to examine the crystal structure of the sample by using a Bede D1 X-ray diffractometer with Cu Kα radiation from 3° to 85° at a rate of 3° min⁻¹. The morphologies were examined by scanning electron microscopy (Hitachi S-4700) with an accelerating voltage of 20 kV and TEM at 200 kV with a JEM-2100F field emission TEM. The compositions of the samples were measured at room temperature by X-ray photoelectron spectroscopy (XPS, ESCALAB250) with a monochromated Al-Mg X-ray source (Al \hbar = 1486.6 eV; Mg \hbar = 1253.6 eV).

2.6. Electrochemical measurements

The electrocatalytic performance of the samples was evaluated by an electrochemical biopotentiostat workstation (CH Instrument, shanghai, China) with a typical three-electrode system. A saturated calomel electrode (SCE) was used as the reference electrode, a glassy carbon electrode (GCE) as the working electrode, and a platinum wire as the counter electrode. The working electrode was modified by the catalyst inks. For the catalyst ink preparation, 5 mg catalyst was dispersed in 1 mL mixture solution of ethanol (950 μL) and Nafion (1 wt%, 50 μL). After sonication for 30 min, the uniform catalyst ink (10 μL) was decorated on the surficial disk of GCE, and a commercially available catalyst 20% Pt/C and 40% IrO₂ supported carbon black were also prepared for comparison under the same method.

Electrochemical measurements for the ORR/OER: Cyclic voltammetry (CV) and linear sweep voltammetry (LSV) measurements from 0 to 1.1 V (vs RHE) was conducted on an electrochemical workstation combined with a rotating disk electrode (RDE) using N₂/O₂-saturated 0.1 M KOH solutions. The ORR in O₂-saturated 0.1 M KOH solution at 1600 rpm was used to evaluate the catalytic performance with a scan rate of 5 mV s⁻¹ from 0 to 1.1 V (vs RHE). The OER performance was studied in O₂-saturated 0.1 M KOH solution with a scan rate of 5 mV s⁻¹ from 0 to 0.8 V at 1600 rpm.

Calculation of HO₂⁻ yield and electron transfer number (*n*): RRDE measurements were performed in O₂-saturated 0.1 M KOH solution with a rotation rate of 1600 rpm and a scan rate of 5 mV s⁻¹. The HO₂⁻ (%) and *n* can be respectively calculated by Eqs. (1) and (2):

$$n = \frac{4I_d}{N(I_d + I_r/N)} \quad (1)$$

$$HO_2^- (\%) = \frac{200I_r}{N(I_d + I_r/N)} \quad (2)$$

where *I_d* is the disk current, *I_r* is the ring current, and *N* is the ring collection efficiency which was provided as 0.37 by manufacturer.

The faradaic efficiency of FeNi-COP-800 catalyst was calculated by Eq. (3), where *j* is current density of oxygen evolution (10 mA cm⁻²). *t* is the time for oxygen evolution. *n* and F are respectively electron transfer number of generating per O₂ molecule (here *n* = 4) and Faraday constant (96485 C mol⁻¹).

$$\text{Faradaic efficiency} = \frac{\text{mole of O}_2 \text{ (measured by GC)}}{j(\text{mA/cm}^2) t(\text{s})/nF} \quad (3)$$

Zinc-air flow battery tests: The zinc-air batteries tests were performed in a homemade zinc-air cell. 2 mg FeNi-COP-800 (or mixture of 1 mg Pt/C and 0.2 mg IrO₂) coated on a carbon paper over a square area 1 cm⁻² to achieve a catalyst loading of 2 mg cm⁻² (or 1.2 mg cm⁻²) and a polished Zn plate was used as the air cathode and anode, respectively. An 8 M KOH and 0.2 M ZnO mixed solution was used as the electrolyte. A Land CT2001A system was used to perform the cycling test at a current density of 5 mA cm⁻². Each discharge and charge period were set to be 1 h. The discharge and charge voltage profiles were collected by two independent Land CT2001 channels alternatively.

3. Results and discussion

3.1. Structural characterization

As shown in Scheme 1, the metal-phthalocyanine-based COPs were synthesized by Schiff-base coupling polymerization. Polymerization of Fe- and Ni-phthalocyanine with terephthalaldehyde produced bimetallic FeNi-COP, while monometallic Fe-COP and Ni-COP were also prepared under the same reaction condition. To confirm a successful polymerization between TA and MePc(NH₂)₄ (Me = Fe, Ni), both FTIR and solid state ¹³C NMR spectroscopy were used to examine the molecular structure of the FeNi-COP. Fig. 1a showed that bands at 3322 cm⁻¹ (-NH₂ stretching) can be attributed to the primary amine group of FePc(NH₂)₄ [45,46], while the aldehyde group of TA at 2870 (C—H stretching) and 1690 cm⁻¹ (C=O stretching) are absent or strongly attenuated in the spectra of FeNi-COP. As can be seen in Solid-state ¹³C NMR spectrum of FeNi-COP (Fig. 1b), chemical shifts in 158, 138, and 129 ppm can be assigned to carbon atoms linked by the imine-bond nitrogen (7, 8), carbon atoms of the pyrrole rings (1) and neighboring the imine bonds (9), and the aromatic carbon atoms (2–6, 10), respectively. The chemical shifts located at 38 and 67 ppm are originated from the synthesis procedure by using THF and DMAc, respectively. The above results indicate that FeNi-COP have been synthesized successfully.

The morphology and microstructure of FeNi-COP and FeNi-COP-800 were characterized by using scanning electron microscopy (SEM) and transmission electron microscopy (TEM). As shown in Fig. S1 and S2, FeNi-COP revealed a sheet-like structure with stack, and the X-ray diffraction (XRD) result for FeNi-COP showed two peaks at 4.82° and 25.4° (Fig. 1c), which are assigned to the (110) and (001) facets, respectively [46]. The crystalline feature probably benefits from the π-π interaction between phthalocyanines to facilitate the building blocks in the stacking direction [47]. On the other hand, the peak at 25.4° implies the interlayer spacing of 3.6 Å in the FeNi-COP [46]. Although the presence of FeNi-COP framework was confirmed, its crystallinity was still limited by the conformational fluctuation at mesoscopic scale [48]. After FeNi-COP transformed into FeNi-COP-800 by 800 °C pyrolysis, the original sheet-stack-like structure transformed into the irregular shape (Fig. S3). Fig. 1d showed the disappearance of the peak at 4.82° in FeNi-COP-800 owing to the destruction of crystalline structure in FeNi-COP via high-temperature pyrolysis, and the peak (002) for the graphitic structure was found at 26.8°, confirming the successful conversion of FeNi-COP into carbon material [49,50]. In addition, metallic particles generated by pyrolysis can be observed in HTEM images (Fig. S4). From the XRD pattern of FeNi-COP-800 (Fig. 1d), the peaks marked by green circles match well with FeNi alloy (PDF#47-1417), while the peaks marked by red triangles can be ascribed to NiFe₂O₄ (PDF#10-0325).

The chemical composition of FeNi-COP-800 was further investigated by the XPS with the survey spectra shown in Fig. 2. Respective atomic contents of C, N, O, Fe and Ni were found to be 82.3%, 5.6%, 9.4%, 0.62% and 0.47%, and the strongest C 1s suggests that carbon is the major element in FeNi-COP-800 catalyst (Fig. 2a). The high resolution N 1s spectrum in Fig. 2b confirmed three types of nitrogen including pyridinic-N/N-Fe at 398.5 eV, graphitic-N at 400.1 eV

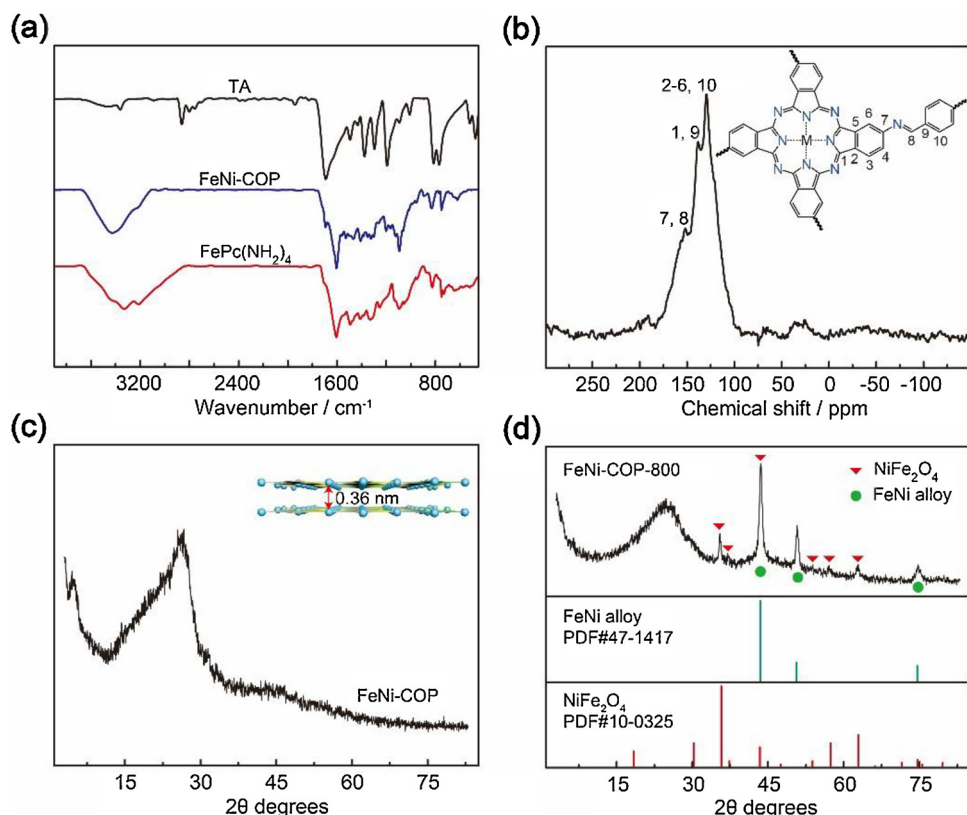


Fig. 1. (a) FTIR spectra of TA, FeNi-COP and FePc(NH₂)₄; (b) Solid-state ¹³C CP MAS NMR spectra of FeNi-COP; (c) XRD patterns for FeNi-COP; (d) XRD patterns for FeNi-COP-800, and standard XRD patterns for FeNi alloy and NiFe₂O₄.

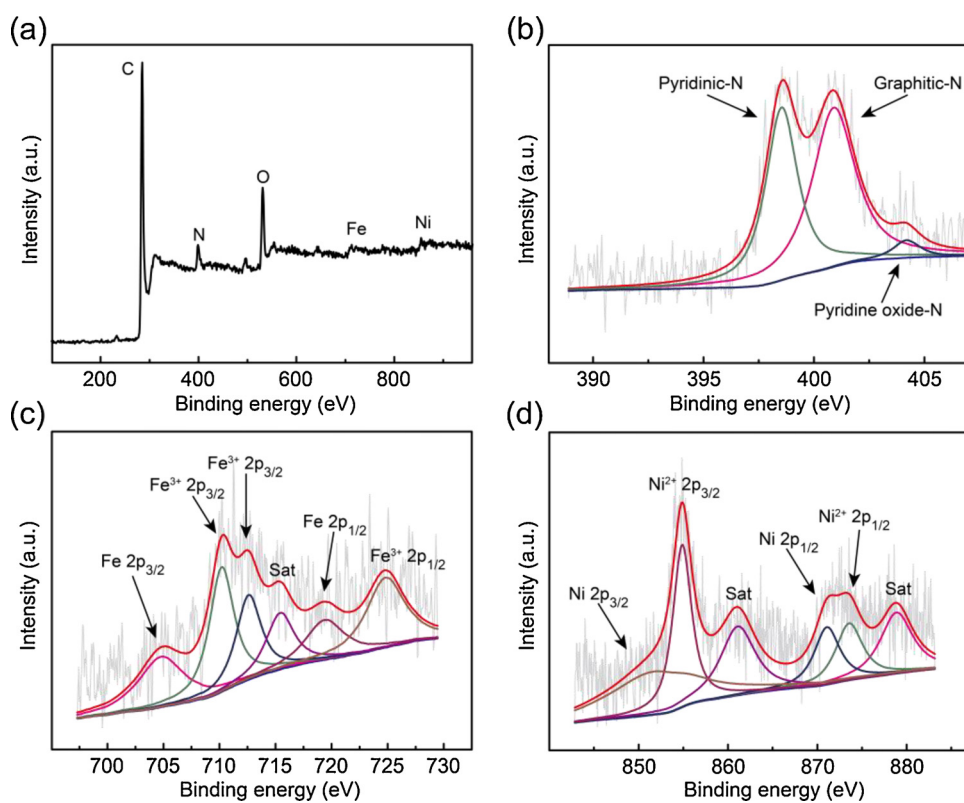


Fig. 2. (a) XPS survey spectra of FeNi-COP-800; (b) high-resolution N 1 s XPS FeNi-COP-800; (c) high-resolution Fe 2p XPS FeNi-COP-800 and (d) high-resolution Ni 2p XPS FeNi-COP-800.

and pyridine oxide-N at 403.8 eV, while the graphitic-N and pyridinic-N were able to adjust the chemical/electronic contexts for neighboring C, thus accelerating the ORR process [39,51,52]. To gain insight into the intrinsic feature of coordination between N/O and transition metal, the Fe 2p spectrum and the Ni 2p spectrum were further deconvoluted. Fig. 2c showed three peaks for Fe^{3+} at 710.3, 712.5, 715.4 and 724.8 eV, implying the coordination between Fe and N/O moieties [53,54], while the peaks at 705.2 and 719.5 eV were assigned to Fe, indicating the existence of Fe phase as also confirmed by the XRD (Fig. 1d). Similarly, in the Ni 2p spectrum, the peaks at 854.7, 873.5 and 878.8 eV are ascribed to Ni^{2+} (Fig. 2d), suggesting that Ni^{2+} species existed in the form of nitrides or oxides [54–56], and the peaks at 852.1, 860.9 and 870.8 eV exhibited the existence of Ni phase (Fig. 2d). Moreover, transition metal (Fe, Co and Ni) and its nitrides/oxides in improving the electrocatalytic performance toward ORR and OER have been largely demonstrated [57–60].

3.2. Electrocatalytic performance

The electrocatalytic performance of FeNi-COP-X for ORR was examined in 0.1 M KOH aqueous solution with a three-electrode system. In order to assess the ORR activity, the CV measurements in N_2 - and O_2 -saturated 0.1 M KOH solution were carried out at a scan rate of 100 mV s^{-1} . As shown in Fig. S5, the FeNi-COP-900 catalyst displayed no noticeable reduction peak in N_2 -saturated electrolyte during the chosen potential range, whereas a notable cathodic peak occurred at 0.725 V in O_2 -saturated environment, displaying an efficient ORR activity of FeNi-COP-900.

To further examine the ORR electrocatalytic activity of FeNi-COP-X catalysts, LSV curves of FeNi-COP-X, Pt/C and IrO_2/C catalysts were performed as presented in Fig. 3a. The onset and half-wave potentials for FeNi-COP-800 (0.955 V and 0.803 V) were close to those for benchmark Pt/C (0.99 V and 0.825 V), and more positive than those for FeNi-COP-700, FeNi-COP-900 and IrO_2/C , respectively, indicating that FeNi-COP-800 possesses a highly efficient ORR electrocatalytic activity. On the other hand, FeNi-COP-800 catalyst possessed the excellent stability in the alkaline system (Fig. S6). Moreover, the Tafel plot for FeNi-COP-800 was higher than those for FeNi-COP-700 and FeNi-COP-900

(Fig. 3b). Subsequently, the catalytic reaction pathway of FeNi-COP-800 was determined by the RRDE. Fig. S7 showed that the ring current for FeNi-COP-800 was much lower than the disk current, while the electron transfer number per O_2 of ORR and the HO_2^- formation on FeNi-COP-800 catalyst were calculated to be 3.85–3.94 and 7.4%–3.1% (Fig. 3c), respectively, in the range from 0.65 V to 0.85 V, which were close to those on Pt/C, clearly indicating a dominant 4-electron transfer pathway for ORR with excellent electrocatalytic selectivity. Additionally, the 4-electron transfer pathway have been reinforced by Koutecky-Levich plots (Fig. S8). As for OER, Fig. 3d revealed that FeNi-COP-800 shared the same potential of 1.63 V at 10 mA cm^{-2} with the OER benchmark IrO_2/C , and FeNi-COP-800 showed the higher diffusion-limiting current density than other catalysts occurred in Fig. 3d. Moreover, both Tafel plot and overpotential at 10 mA cm^{-2} for FeNi-COP-800 were very close to those for IrO_2/C (Fig. 3e and 3 f), implying that FeNi-COP-800 exhibits superior electrocatalytic activity and IrO_2 -like kinetic process for OER. On the other hand, the OER performance and stability of FeNi-COP-800 in 1.0 M KOH have been also investigated as shown in Fig. S9, while the faradaic efficiency have been calculated as 94.2% from Fig. S10. The results above also suggested the optimal pyrolysis temperature at 800 °C for obtaining the higher ORR and OER performance.

3.3. Effect of pyrolysis temperature for ORR/OER activity

In order to understand the effect of the pyrolysis temperature on ORR and OER performance for FeNi-COP-X, the FeNi-COP-X were also characterized by XRD and Raman spectra. As presented in Fig. S11, more peaks can be occurred with increasing the pyrolysis temperature from 700 to 900 °C, and the peaks for FeNi alloy and NiFe_2O_4 in FeNi-COP-700 were featureless, suggesting metallic particles easier formed in higher pyrolysis temperature. After acid-treatment in FeNi-COP-800, the metallic particles in FeNi-COP-800 were decreasing with decreasing electrocatalytic activity (Fig. S12, S13 and S14), which is consistent with our previous study that metallic particle could efficiently enhance the electrocatalytic activity of the catalysts [61]. Thus the above results reasonably explained why the electrocatalytic activity for FeNi-COP-700 is inferior to those for FeNi-COP-800 and –900. Furthermore,

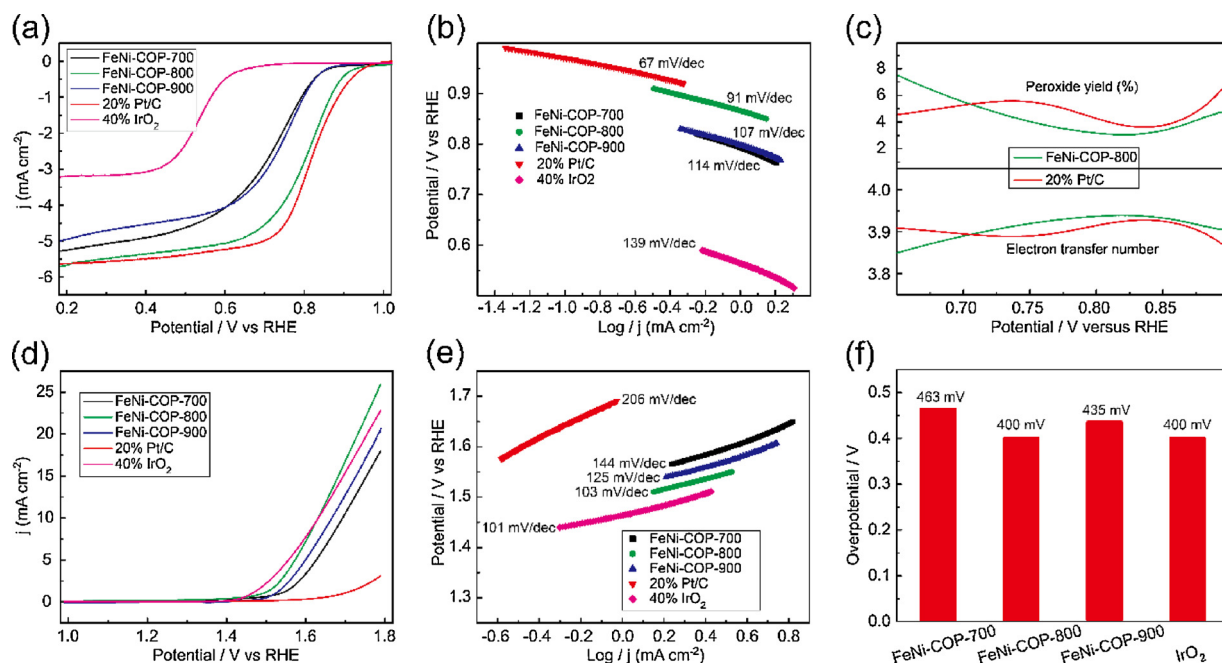


Fig. 3. (a) ORR LSV curves and (b) Tafel plots of FeNi-COP-X, 20% Pt/C and 40% IrO_2/C ; (c) electron transfer number and peroxide yield of the FeNi-COP-800 and 20% Pt/C. (d) OER LSV curves, (e) Tafel plots and (f) overpotential of FeNi-COP-X, 20% Pt/C and 40% IrO_2/C . All the LSV curves were tested in O_2 -saturated 0.1 M KOH solution at a scan and rotation rates of 5 mV s^{-1} and 1600 rpm.

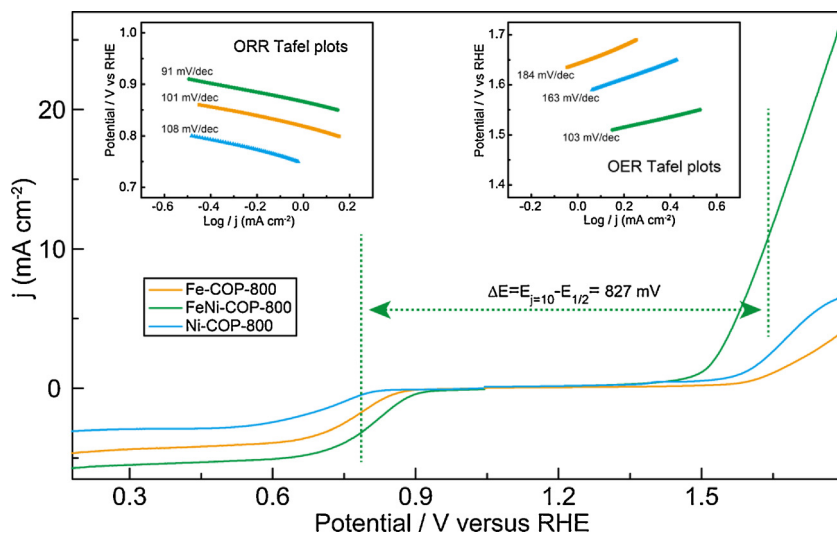


Fig. 4. The overall LSV curves of Fe-COP-800, FeNi-COP-800 and Ni-COP-800. Inset: ORR Tafel plots (left) and OER Tafel plots (right). All the LSV curves were tested in O_2 -saturated 0.1 M KOH solution at a scan and rotation rates of 5 mV s^{-1} and 1600 rpm, respectively.

Raman spectra was used to record the typical peaks at 1341 and 1580 cm^{-1} , which are in accordance with the defect mode (D-band) and E_{2g} mode (G-band) [62]. As shown in Fig. S15, the I_D/I_G ratio for FeNi-COP-800 is higher than those for FeNi-COP-700 and -900, indicating that more defects and exposed active sites for ORR and OER were created at 800°C , therefore, FeNi-COP-800 holds better ORR and OER activities among the FeNi-COP-X (X = 700 and 900).

3.4. Tunable ORR/OER activity by tailoring building units in Fe/Ni-COP electrocatalysts

According to the optimal pyrolysis temperature (800°C), the catalytic activities toward ORR and OER were further investigated by tuning the components of Fe/Ni-COP-800 through tailoring the building units in COPs. Here, Fe- and Ni-phthalocyanine were selected to prepare the monometal- and bimetal-catalysts including Fe-, Ni- and FeNi-COP-800, while the catalysts (marked as FePc-800, NiPc-800 and Mixed FeNiPc-800) derived from a non-polymerized Fe- (or Ni-) phthalocyanine and a physical mixture of Fe- and Ni-phthalocyanine was also prepared for comparison. As shown in Fig. 4, the ORR and OER performance for FeNi-COP-800 is apparently better than those for Fe- and Ni-COP-800, and both lower ORR and OER Tafel plots in FeNi-COP-800 implied more efficient ORR/OER kinetic process among Fe- and Ni-COP-800 catalysts. Furthermore, FeNi-COP-800 gave a ΔE of 827 mV (Fig. 4) that surpassed many reported promising bifunctional materials (listed in Table S1). On the other hand, Mixed FeNiPc-800 show improved activity among FePc-800 and NiPc-800, but the corresponding catalysts such as Mixed FeNiPc-800 obtained by non-polymerized precursors still exhibited lower ORR/OER performance than those catalysts like FeNi-COP-800 originating from precursors with polymerized network structure (Fig. S16), which was triggered by the metal species, occurred in catalysts derived from precursors without polymerized network structure, easier aggregating into bigger particles and further prevented the metal species from well-distributing in the carbon matrix (Fig. S17), implying the significant effect of the COP-network on the enhanced ORR/OER electrocatalytic activities. Therefore, the results mentioned above suggest that FeNi-COP-800 possesses superior bi-functional activities for both OER and ORR, and the enhanced bi-electrocatalytic activities of FeNi-COP-800 are closely associated with the coexistence of Fe and Ni elements in the FeNi-COP-800.

3.5. Practical evaluation in homemade zinc-air flow battery

Considering the electrocatalytic stability of FeNi-COP-800, both the homemade zinc-air flow (Fig. 5) battery and solid zinc-air battery (Fig. S18) were assembled to further investigate their performance in practical operation condition. As can be seen in Fig. 5a, the maximum power density of the battery using FeNi-COP-800 (64 mW cm^{-2}) exhibits higher than that of benchmark Pt/C (56 mW cm^{-2}) (Fig. 5b). Moreover, long-term cycling test show low voltage change in FeNi-COP-800 over 175 h (Fig. 5c and Fig. S19), while the voltage efficiency of FeNi-COP-800 catalyst decreased from initial 55.8% to 52.9% after 175 h , and the loss of the voltaic efficiency is only 2.9% (Fig. 5d), which were better to those of Pt/C (voltage attenuation from 48.7% to 44.2% and 4.5% loss of voltage efficiency) (Fig. 5d), suggesting a superior stability of FeNi-COP-800 for ORR and OER. Therefore, it is reasonable to conclude that the molecular rational design in precursors by appropriately selecting the building units with desired components for COP is able to serve the desired catalysts with bi/multi-active sites for efficient/stable ORR and OER performance.

4. Conclusion

In summary, we reported a facile but efficient approach to prepare constituent-tunable Fe-Ni heteroatom carbon-based catalysts for oxygen electrode via tailorabile metal-phthalocyanine-based covalent organic polymers as self-sacrificial precursors. A highly efficient FeNi-COP-800 electrocatalyst derived from a FeNi-COP precursor was prepared for oxygen electrode. The as-prepared FeNi-COP-800 exhibits an efficient ORR performance with a half-potential of 0.803 V as well as an IrO_2 -like OER activity with a potential of 1.63 V at 10 mA cm^{-2} , which surpass those of Fe-COP-800 and Ni-COP-800. Moreover, a homemade zinc-air flow battery comprising FeNi-COP-800 catalyst shows a power density of 64 mW cm^{-2} and superior stability with 2.9% potential loss after 85 cycles in 175 h of practical operation. Accordingly, this work on appropriately tailoring the building units with desired components in COP precursors might provide a simple way in designing and fabricating catalysts with unique structure and multi-active sites for multi-functional electrocatalysis.

Acknowledgment

This work was supported by Beijing Natural Science Foundation (17L20060; 2162032); NSF of China (51502012; 21676020;

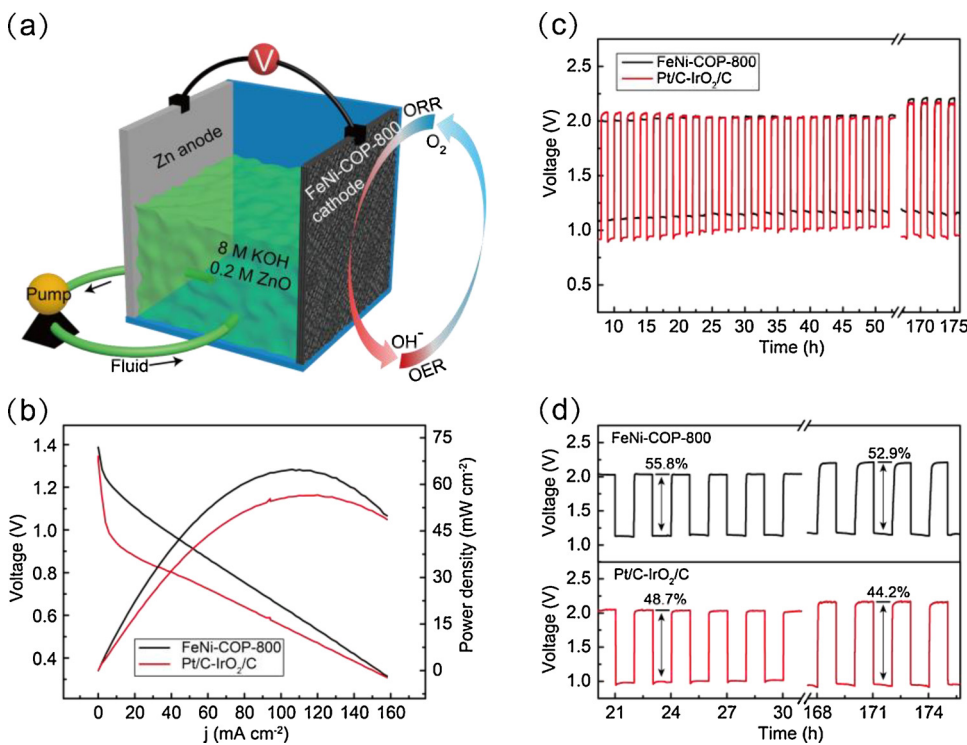


Fig. 5. (a) Scheme of the Zn-air flow battery. (b) Discharge polarization curves and corresponding power density plots; (c) Charge-discharge cycling performance of the Zn-air flow batteries based on FeNi-COP-800 and Pt/C-IrO₂/C catalysts at a constant charge-discharge current density of 5 mA cm^{-2} ; (d) Voltaic efficiency of the Zn-air flow batteries using FeNi-COP-800 and Pt/C-IrO₂/C.

21606015); The Start-up fund for talent introduction of Beijing University of Chemical Technology (buctrc201420, buctrc201714); Talent cultivation of State Key Laboratory of Organic-Inorganic Composites; The Fundamental Research Funds for the Central Universities (ZD1502; buctrc201524); Distinguished scientist program at BUCT (buctylkjxj02); The “111” project of China (B14004).

Appendix A. Supplementary data

Supplementary data associated with this article can be found, in the online version, at <https://doi.org/10.1016/j.apcatb.2018.10.038>.

References

- [1] I.S. Amiinu, X. Liu, Z. Pu, W. Li, Q. Li, J. Zhang, H. Tang, H. Zhang, S. Mu, *Adv. Funct. Mater.* 28 (2018) 1704638–1704646.
- [2] S. Li, C. Cheng, X. Zhao, J. Schmidt, A. Thomas, *Angew. Chem. Int. Ed.* 57 (2018) 1856–1862.
- [3] J. Lv, S.C. Abbas, Y. Huang, Q. Liu, M. Wu, Y. Wang, L. Dai, *Nano Energy* 43 (2018) 130–137.
- [4] Z. Pei, H. Li, Y. Huang, Q. Xue, Y. Huang, M. Zhu, Z. Wang, C. Zhi, *Energy. Environ. Sci.* 10 (2017) 742–749.
- [5] S.S. Shinde, C.H. Lee, J.Y. Yu, D.H. Kim, S.U. Lee, J.H. Lee, *ACS Nano* 12 (2018) 596–608.
- [6] M. Wang, T. Qian, J. Zhou, C. Yan, *ACS Appl. Mater. Inter.* 9 (2017) 5213–5221.
- [7] S. Zhao, L. Yan, H. Luo, W. Mustain, H. Xu, *Nano Energy* 47 (2018) 172–198.
- [8] G.R. Zhang, S. Woellner, *Appl. Catal. B-Environ.* 222 (2018) 26–34.
- [9] P. Cai, Y. Hong, S. Ci, Z. Wen, *Nanoscale* 8 (2016) 20048–20055.
- [10] Z. Ma, K. Wang, Y. Qiu, X. Liu, C. Cao, Y. Feng, P. Hu, *Energy* 143 (2018) 43–55.
- [11] Z. Zhao, Z. Xia, *ACS Catal.* 6 (2016) 1553–1558.
- [12] J. Ying, J. Li, G. Jiang, Z.P. Cano, Z. Ma, C. Zhong, D. Su, Z. Chen, *Appl. Catal. B-Environ.* 225 (2018) 496–503.
- [13] C. Gutsche, C.J. Moeller, M. Knipper, H. Borchert, J. Parisi, T. Plaggenborg, *J. Phys. Chem. C* 120 (2016) 1137–1146.
- [14] A. Pavlisic, P. Jovanovic, V.S. Selih, M. Sala, M. Bele, G. Drazic, I. Arcon, S. Hocevar, A. Kokalj, N. Hodnik, M. Gabersek, *ACS Catal.* 6 (2016) 5530–5534.
- [15] S. Yang, Y.J. Tak, J. Kim, A. Soon, H. Lee, *ACS Catal.* 7 (2017) 1301–1307.
- [16] A. Zubiaur, N. Job, *Appl. Catal. B-Environ.* 225 (2018) 364–378.
- [17] Y. Qian, Z. Hu, X. Ge, S. Yang, Y. Peng, Z. Kang, Z. Liu, J.Y. Lee, D. Zhao, *Carbon* 111 (2017) 641–650.
- [18] T. Wang, Z. Kou, S. Mu, J. Liu, D. He, I.S. Amiinu, W. Meng, K. Zhou, Z. Luo, S. Chaemchuen, F. Verpoorten, *Adv. Funct. Mater.* 28 (2018) 1705048–1705056.
- [19] Y. Qian, T. An, K.E. Birgersson, Z. Liu, D. Zhao, *Small* 14 (2018) 1704169–1704178.
- [20] H. Zhang, H. Osgood, X. Xie, Y. Shao, G. Wu, *Nano Energy* 31 (2017) 331–350.
- [21] C. Zhu, S. Fu, J. Song, Q. Shi, D. Su, M.H. Engelhard, X. Li, D. Xiao, L. Estevez, D. Du, Y. Lin, *Small* 13 (2017) 1603407–1603413.
- [22] J.H. Kim, D.H. Youn, K. Kawashima, J. Lin, H. Lim, C.B. Mullins, *Appl. Catal. B-Environ.* 225 (2018) 1–7.
- [23] Y. Li, M. Zhao, Y. Zhao, L. Song, Z. Zhang, *Part. Part. Syst. Char.* 33 (2016) 158–166.
- [24] N.T. Suen, S.F. Hung, Q. Quan, N. Zhang, Y.J. Xu, H.M. Chen, *Chem. Soc. Rev.* 46 (2017) 337–365.
- [25] C. Wei, Z. Feng, G.G. Scherer, J. Barber, Y. Shao-Horn, Z.J. Xu, *Adv. Mater.* 29 (2017) 1606800–1606807.
- [26] J. Yin, Y. Li, F. Lv, Q. Fan, Y.Q. Zhao, Q. Zhang, W. Wang, F. Cheng, P. Xi, S. Guo, *ACS Nano* 11 (2017) 2275–2283.
- [27] X. Han, X. Wu, C. Zhong, Y. Deng, N. Zhao, W. Hu, *Nano Energy* 31 (2017) 541–550.
- [28] Z. Li, M. Shao, Q. Yang, Y. Tang, M. Wei, D.G. Evans, X. Duan, *Nano Energy* 37 (2017) 98–107.
- [29] Q. Wang, L. Shang, R. Shi, X. Zhang, G.I.N. Waterhouse, L.Z. Wu, C.H. Tung, T. Zhang, *Nano Energy* 40 (2017) 382–389.
- [30] H. Osgood, S.V. Devaguptapu, H. Xu, J. Cho, G. Wu, *Nano Today* 11 (2016) 601–625.
- [31] Q. Xiang, F. Li, W. Chen, Y. Ma, Y. Wu, X. Gu, Y. Qin, P. Tao, C. Song, W. Shang, H. Zhu, T. Deng, J. Wu, *ACS Energy Lett.* 3 (2018) 2357–2365.
- [32] S. Cai, Z. Meng, H. Tang, Y. Wang, P. Tsakaratas, *Appl. Catal. B-Environ.* 217 (2017) 477–484.
- [33] T. Cao, D. Wang, J. Zhang, C. Cao, Y. Li, *Chem. Eur. J.* 21 (2015) 14022–14029.
- [34] D. He, Y. Xiong, J. Yang, X. Chen, Z. Deng, M. Pan, Y. Li, S. Mu, *J. Mater. Chem. A* 5 (2017) 1930–1934.
- [35] B. Li, Y. Chen, X. Ge, J. Chai, X. Zhang, T.S.A. Hor, G. Du, Z. Liu, H. Zhang, Y. Zong, *Nanoscale* 8 (2016) 5067–5075.
- [36] W. Li, W. Ding, G. Wu, J. Liao, N. Yao, X. Qi, L. Li, S. Chen, Z. Wei, *Chem. Eng. Sci.* 135 (2015) 45–51.
- [37] L. Chen, L. Zhang, Z. Chen, H. Liu, R. Luque, Y. Li, *Chem. Sci.* 7 (2016) 6015–6020.
- [38] Y. Su, Z. Yao, F. Zhang, H. Wang, Z. Mics, E. Canovas, M. Bonn, X. Zhuang, X. Feng, *Adv. Funct. Mater.* 26 (2016) 5893–5902.
- [39] J. Guo, M. Ning, Z. Xiang, *J. Energy Chem.* 26 (2017) 1168–1173.
- [40] P. Peng, Z. Zhou, J. Guo, Z. Xiang, *ACS Energy Lett.* 2 (2017) 1308–1314.
- [41] Z. Xiang, Y. Xue, D. Cao, L. Huang, J.F. Chen, L. Dai, *Angew. Chem. Int. Edit.* 53 (2014) 2433–2437.
- [42] Q. Lin, X. Bu, A. Kong, C. Mao, F. Bu, P. Feng, *Adv. Mater.* 27 (2015) 3431–3436.
- [43] Z. Xiang, D. Cao, L. Dai, *Polym. Chem.* 6 (2015) 1896–1911.
- [44] P.J. Waller, F. Gandara, O.M. Yaghi, *Accounts Chem. Res.* 48 (2015) 3053–3063.
- [45] X. Ding, B.H. Han, *Angew. Chem. Int. Edit.* 54 (2015) 6536–6539.
- [46] N. Huang, L. Zhai, H. Xu, D. Jiang, *J. Am. Chem. Soc.* 139 (2017) 2428–2434.
- [47] G. Lin, H. Ding, R. Chen, Z. Peng, B. Wang, C. Wang, *J. Am. Chem. Soc.* 139 (2017) 8705–8709.
- [48] J. He, N. Wang, Z. Cui, H. Du, L. Fu, C. Huang, Z. Yang, X. Shen, Y. Yi, Z. Tu, Y. Li, *Nat. Commun.* 8 (2017) 1172–1182.
- [49] Z. Wang, Y. Lu, Y. Yan, T.Y.P. Larissa, X. Zhang, D. Wuu, H. Zhang, Y. Yang, X. Wang, *Nano Energy* 30 (2016) 368–378.
- [50] Z. Zhang, M. Dou, H. Liu, L. Dai, F. Wang, *Small* 12 (2016) 4193–4199.

[51] J. Guo, Y. Li, Y. Cheng, L. Dai, Z. Xiang, ACS Nano 11 (2017) 8379–8386.

[52] S.B. Ren, J. Wang, X.H. Xia, ACS Appl. Mater. Inter. 8 (2016) 25875–25880.

[53] Q. Zuo, P. Zhao, W. Luo, G. Cheng, Nanoscale 8 (2016) 14271–14277.

[54] Z. Wang, M. Li, L. Fan, J. Han, Y. Xiong, Appl. Surf. Sci. 401 (2017) 89–99.

[55] Y. Fan, S. Iida, A. Staykov, T. Akbay, H. Hagiwara, J. Matsuda, K. Kaneko, T. Ishihara, Small 13 (2017) 1700099–1700106.

[56] G. Fu, Z. Cui, Y. Chen, Y. Li, Y. Tang, J.B. Goodenough, Adv. Energy Mater. 7 (2017) 1601172–1601179.

[57] Y. Cheng, S. Dou, J.P. Veder, S. Wang, M. Saunders, S.P. Jiang, ACS Appl. Mater. Inter. 9 (2017) 8121–8133.

[58] J. Fang, L. Hu, M. Wang, L. Gan, C. Chen, Y. Jiang, B. Xiao, Y. Lai, J. Li, Mater. Lett. 218 (2018) 36–39.

[59] Q. Wang, L. Shang, R. Shi, X. Zhang, Y. Zhao, G.I.N. Waterhouse, L.Z. Wu, C.H. Tung, T. Zhang, Adv. Energy Mater. 7 (2017) 1700467–1700473.

[60] N.I. Andersen, A. Serov, P. Atanassov, Appl. Catal. B-Environ. 163 (2015) 623–627.

[61] J. Guo, Y. Cheng, Z. Xiang, ACS Sustain. Chem. Eng. 5 (2017) 7871–7877.

[62] D. Yan, Y. Li, J. Huo, R. Chen, L. Dai, S. Wang, Adv. Mater. 29 (2017) 1606459–1606478.